

## Quantum criticality in heavy-fermion metals

Philipp Gegenwart, Qimiao Si, Frank Steglich

### Angaben zur Veröffentlichung / Publication details:

Gegenwart, Philipp, Qimiao Si, and Frank Steglich. 2008. "Quantum criticality in heavy-fermion metals." *Nature Physics* 4 (3): 186–97.  
<https://doi.org/10.1038/nphys892>.

### Nutzungsbedingungen / Terms of use:

licgercopyright

Dieses Dokument wird unter folgenden Bedingungen zur Verfügung gestellt: / This document is made available under the following conditions:

**Deutsches Urheberrecht**

Weitere Informationen finden Sie unter: / For more information see:

<https://www.uni-augsburg.de/de/organisation/bibliothek/publizieren-zitieren-archivieren/publizieren>



# Quantum criticality in heavy-fermion metals

Quantum criticality describes the collective fluctuations of matter undergoing a second-order phase transition at zero temperature. Heavy-fermion metals have in recent years emerged as prototypical systems to study quantum critical points. There have been considerable efforts, both experimental and theoretical, that use these magnetic systems to address problems that are central to the broad understanding of strongly correlated quantum matter. Here, we summarize some of the basic issues, including the extent to which the quantum criticality in heavy-fermion metals goes beyond the standard theory of order-parameter fluctuations, the nature of the Kondo effect in the quantum-critical regime, the non-Fermi-liquid phenomena that accompany quantum criticality and the interplay between quantum criticality and unconventional superconductivity.

PHILIPP GEGENWART<sup>1</sup>, QIMIAO SI<sup>2\*</sup>  
AND FRANK STEGLICH<sup>3</sup>

<sup>1</sup>I. Physik. Institut, Georg-August Universität Göttingen,  
D-37077 Göttingen, Germany

<sup>2</sup>Department of Physics and Astronomy, Rice University, Houston,  
Texas 77005, USA

<sup>3</sup>Max-Planck-Institut für Chemische Physik fester Stoffe,  
D-01187 Dresden, Germany

\*e-mail: qmsi@rice.edu

In the classical world, matter in equilibrium freezes at absolute zero temperature. A macroscopic collection of microscopic particles adopts a stationary arrangement, forming an ordered pattern, to minimize the potential energy. Quantum mechanics, on the other hand, allows fluctuations even at zero temperature. The effective strength of such zero-point motion can be tuned through the variation of a non-thermal control parameter, such as applied pressure. When such quantum fluctuations become sufficiently strong, the system undergoes a quantum phase transition to a new ground state.

As simple as this sounds, quantum phase transitions are not easy to achieve. Consider, for example, the case of ice. Anybody who has skated would appreciate the fact that the melting temperature of ice is reduced by pressure. If the melting temperature were forced to vanish at a sufficiently high pressure, a quantum phase transition would take place at this pressure. However, applying pressure larger than about 0.2 GPa to ice actually makes the melting temperature go up again<sup>1</sup>.

The transformation between ice and water also illustrates another concept in phase transitions. At the melting point, ice abruptly turns into water, absorbing latent heat. In other words, the transition is of first order. A piece of magnet, on the other hand, typically ‘melts’ into a paramagnet through a continuous transition: the magnetization vanishes smoothly, and no latent heat is involved. In the case of zero temperature, the point of such a second-order phase transition is the quantum critical

point (QCP)<sup>2,3</sup>. The quantum-critical state is distinct from the phases on both sides, and is expected to show features in its physical properties that are universal. Moreover, it will contain emergent low-energy excitations that are highly collective, thereby representing a quantum state of matter with properties that are necessarily different from those of any weakly interacting system.

It was not until recent years that QCPs were experimentally observed<sup>4,5</sup>. Particularly clear-cut examples have come from heavy-fermion (HF) metals, rare-earth-based intermetallic compounds in which the effective charge-carrier masses are hundreds of times the bare-electron mass. Accompanying the large effective electron mass is the fact that the relevant energy scales in the HF metals are so small that their ground states can be readily tuned not only by chemical doping but also through a range of pressure or magnetic field accessible in many condensed-matter physics laboratories.

Two examples best illustrate the observation of QCPs in HF metals. In  $\text{CeCu}_{6-x}\text{Au}_x$  (refs 6,7), Au doping turns the paramagnetic metal phase of the pure  $\text{CeCu}_6$  into an antiferromagnetic (AF) metal phase for  $x > 0.1$  (Fig. 1a). As a function of the doping concentration, the AF transition temperature ( $T_N$ ) sets in continuously; the same applies to the low-temperature staggered moment—spatially modulated magnetization at the AF wavevector. These features establish the existence of an AF QCP. In  $\text{YbRh}_2\text{Si}_2$ , nature is even kinder because the magnetic transition temperature is as low as 70 mK in the parent undoped compound<sup>8</sup>. The magnetic ordering is continuously suppressed by the application of a small magnetic field, leading to a field-driven AF QCP. Of course, measurements can never be extended down to zero temperature. Our statement about the continuous nature of the transition is made on the basis of the understanding that the lowest measured temperature, 50 mK and 20 mK in  $\text{CeCu}_{6-x}\text{Au}_x$  ( $x \geq 0.1$ ) and  $\text{YbRh}_2\text{Si}_2$  respectively, is sufficiently low. (This is to be compared with the upper temperature limit of the quantum-critical scaling regime, which is about 5 K and 10 K in the two systems, respectively.) Similar understanding is assumed when related statements are made henceforth.

The explicit identification of the QCPs in these and related HF metals has in turn helped to establish a number of properties that are broadly important for the physics of strongly correlated electron systems. One of the modern themes, central to a variety of strongly correlated electron systems, is how the standard theory of metals, Landau's Fermi-liquid (FL) theory, can break down (see below, first section). Quantum criticality, through its emergent excitations, serves as a mechanism for NFL behaviour, as demonstrated by a  $T$ -linear electrical resistivity (Fig. 1b,c). Moreover, the NFL behaviour covers a surprisingly large part of the phase diagram. For instance, in Ge-doped YbRh<sub>2</sub>Si<sub>2</sub>, the  $T$ -linear electrical resistivity extends over three decades of temperature (Fig. 1c), a range that contains a large entropy (see below). Finally, quantum criticality can lead to novel quantum phases such as unconventional superconductivity (Fig. 1d).

These experiments have mostly taken place over the past decade, and they have been accompanied by extensive theoretical studies. The latter have led to two classes of quantum criticality for HF metals. One type extends the standard theory of second-order phase transitions to the quantum case<sup>9–11</sup>, whereas the other type invokes new critical excitations that are inherently quantum mechanical<sup>12–14</sup>. The purpose of this article is to provide a status report on this rapidly developing subject.

## MAGNETIC HF METALS AND FL BEHAVIOUR

HF phenomena were first observed in the low-temperature thermodynamic and transport properties of CeAl<sub>3</sub> in 1975 (ref. 15). The 1979 discovery of superconductivity in CeCu<sub>2</sub>Si<sub>2</sub> (ref. 16) made HF physics a subject of extensive studies. This discovery was initially received by the community with strong scepticism, which, however, was gradually overcome with the aid of two observations, of (1) bulk superconductivity in high-quality CeCu<sub>2</sub>Si<sub>2</sub> single crystals<sup>17</sup> and (2) HF superconductivity in several U-based intermetallics: UBe<sub>13</sub> (ref. 18), UPt<sub>3</sub> (ref. 19) and URu<sub>2</sub>Si<sub>2</sub> (ref. 20; W. Schlabit, *et al.*, unpublished). Around the same time, it was recognized that CeCu<sub>2</sub>Si<sub>2</sub>, CeAl<sub>3</sub> and other Ce-based compounds behaved as 'Kondo-lattice' systems<sup>21</sup>.

### KONDO EFFECT

Consider a localized magnetic moment of spin  $\hbar/2$  immersed in a band of conduction electrons. The Kondo interaction—an exchange coupling between the local moment and the spins of the conduction electrons—is AF. It is energetically favourable for the two types of spin to form an up-down arrangement: when the local moment is in its up state,  $|\uparrow\rangle$ , a linear superposition of the conduction-electron orbitals will be in its down state,  $|\downarrow\rangle_c$ , and vice versa. The correct ground state is not either of the product states, but an entangled state—the Kondo singlet,  $(1/2)(|\uparrow\rangle|\downarrow\rangle_c - |\downarrow\rangle|\uparrow\rangle_c)$ . One of the remarkable features is that there is a Kondo resonance in the low-lying many-body excitation spectrum. The singlet formation in the ground state turns a composite object, formed out of the local moment and a conduction electron, into an elementary excitation with internal quantum numbers that are identical to those of a bare electron—spin  $\hbar/2$  and charge  $e$ . Loosely speaking, because of the entanglement of the local moment with the spin degree of freedom of a conduction electron, the local moment has acquired all the quantum numbers of the latter and is transformed into a composite fermion. We will use the term Kondo effect to describe the phenomenon of Kondo-resonance formation at low temperatures.

At high temperatures, on the other hand, the system wants to maximize the entropy by sampling all of the possible configurations. It gains free energy by making the local moment essentially free, which in turn weakly scatters the conduction

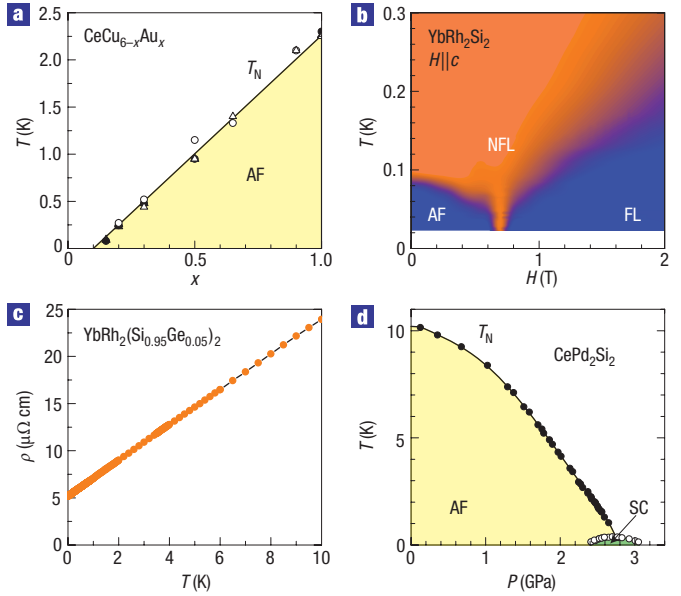


**Figure 1** Quantum critical points in HF metals. **a**, AF ordering temperature  $T_N$  versus Au concentration  $x$  for  $\text{CeCu}_{6-x}\text{Au}_x$  (ref. 7), showing a doping-induced QCP. **b**, Suppression of the magnetic ordering in  $\text{YbRh}_2\text{Si}_2$  by a magnetic field. Also shown is the evolution of the exponent  $\alpha$  in  $\Delta\rho \equiv [\rho(T) - \rho_0] \propto T^\alpha$ , within the temperature–field phase diagram of  $\text{YbRh}_2\text{Si}_2$  (ref. 55). Blue and orange regions mark  $\alpha = 2$  and 1, respectively. **c**, Linear temperature dependence of the electrical resistivity for Ge-doped  $\text{YbRh}_2\text{Si}_2$  over three decades of temperature (ref. 55), demonstrating the robustness of the non-Fermi-liquid (NFL) behaviour in the quantum-critical regime. **d**, Temperature-versus-pressure phase diagram for  $\text{CePd}_2\text{Si}_2$ , illustrating the emergence of a superconducting phase centred around the QCP. The Néel ( $T_N$ ) and superconducting ( $T_c$ ) ordering temperatures are indicated by filled and open symbols, respectively<sup>79</sup>.

electrons; this is the regime of asymptotic freedom, a notion that also plays a vital role in quantum chromodynamics. It is in this regime that Kondo discovered logarithmically divergent correction terms in the scattering amplitude beyond the Born approximation<sup>22</sup>. Kondo's work opened a floodgate to a large body of theoretical work<sup>23</sup>, which, among other things, led to a complete understanding of the crossover between the high-temperature weak-scattering regime and the low-temperature Kondo-singlet state. This crossover occurs over a broad temperature range, and is specified by a Kondo temperature; the latter depends on the Kondo interaction and the density of states of the conduction electrons at the Fermi energy. We will use Kondo screening to refer to the process of developing the Kondo singlet correlations as temperature is lowered.

### KONDO LATTICE AND HEAVY FERMION LIQUID

HF metals contain a lattice of strongly correlated  $f$  electrons and some bands of conduction electrons. The  $f$  electrons are associated with the rare-earth or actinide ions and are, by themselves, in a Mott-insulating state: the on-site Coulomb repulsion is so much stronger than the kinetic energy that these  $f$  electrons behave as localized magnetic moments, typically at room temperature and below. They are coupled to the conduction electrons via an (AF) Kondo interaction. In theoretical model studies, only one band of conduction electrons is typically considered. Such a coupled system is called a Kondo lattice.

It is useful to compare the HF metals with other strongly correlated electron systems. The Mott-insulating nature of the  $f$

electrons not only provides the connection to the single-impurity Kondo problem, but also highlights the similarity between the HF metals and doped Mott insulators occurring in transition metal oxides—such as high-temperature superconductors. The main difference between the HF metals and the doped Mott insulators lies in the way the itinerant charge carriers are introduced to cause delocalization of the  $f$  or  $d$  electrons. In HF metals, delocalization of the Mott-insulating  $f$  electrons arises owing to their coupling to separate bands of conduction electrons. In transition-metal oxides, it is common to think of such a delocalization of  $d$  electrons in terms of the addition/removal of electrons onto/from the transition-metal sites of the Mott insulator.

Historically, the HF metals started out as a fertile ground to study strongly correlated FLs and superconductors<sup>21</sup>. FL theory describes an interacting electron system in terms of Landau quasiparticles, that is, dressed electrons that are adiabatically connected to bare electrons when the electron–electron interactions are adiabatically turned off. These quasiparticles are long lived at low energies, and have the same internal quantum numbers as bare electrons.

In a Kondo lattice, as in a single-impurity Kondo problem, the entanglement in the Kondo-singlet ground state leads to Kondo resonances, which constitute the Landau quasiparticles of the resulting FL state<sup>23</sup>. In this way, the local moments should be counted in the Fermi volume, and the corresponding Fermi surface is ‘large’<sup>23</sup>. The quasiparticles have a heavy mass: after all, they come from magnetic moments which were spatially localized in the absence of the Kondo effect. They also experience some residual interactions, described by the Landau parameters. From a theoretical point of view, the strongly correlated FL state of a Kondo lattice has served as a testing ground for many-body methods—a very successful recent one being the dynamical mean-field theory<sup>24</sup>.

The most common characteristics of an FL state in a clean metal include a  $T^2$  term as the leading temperature dependence of the electrical resistivity  $\Delta\rho (= \rho(T) - \rho_0)$ , and a  $T$ -linear term as the leading temperature dependence of the electronic specific heat. By enhancing the amplitude of these terms, the large carrier mass makes it much easier to observe these FL properties in HF metals than in simple metals and transition-metal compounds.

#### TOWARDS QUANTUM CRITICALITY IN HF METALS

In addition to the Kondo interaction, there also exists the Ruderman–Kittel–Kasuya–Yoshida (RKKY) interaction between the local moments. At the level of energetics, the interplay between these two kinds of interaction was emphasized early on<sup>25,26</sup>. Doniach, in particular, considered a Kondo-lattice model that is simplified in several ways: it lives in one dimension and deals with a purely insulating case—the conduction-electron band is replaced by a lattice of coupled localized spins<sup>25</sup>. On the basis of the relative energies, he concluded that this model has a second-order quantum phase transition: the ground state is an insulating paramagnet when the Kondo interaction dominates over the RKKY interaction, and an insulating antiferromagnet when the RKKY interaction is larger instead. Years later, we have understood that some of the quantum fluctuation effects, which are especially strong in one dimension and ignored in the initial treatment, would in fact lead to a very different phase diagram for the particular one-dimensional model. Still, the competition between the two types of interaction in any Kondo-lattice model is by now well established to be an important microscopic ingredient of HF systems.

Some of the earliest clues pointing to the potential failure of the FL description came from certain alloyed HF materials<sup>27,28</sup>. However, it is the study of the (nearly) stoichiometric HF metals that has provided the direct linkage between NFL phenomenology and quantum criticality.

It is perhaps appropriate to consider the study of quantum criticality, following that of superconductivity, as the second revolution of the HF field. HF metals have been used as a model setting to study QCPs and have elucidated the richness of quantum criticality. At the same time, the notion of quantum criticality is forcing us to revisit some of the age-old questions about HF physics *per se*, including the emergence of heavy quasiparticles and the interplay between magnetism and superconductivity.

#### NATURE OF QUANTUM CRITICALITY

How do we theoretically describe quantum criticality? In Landau’s theory of phase transitions, phases are distinguished in terms of an order parameter, which characterizes symmetry breaking. For instance, a staggered magnetization differentiates between an antiferromagnet and a paramagnet. At a second-order phase transition, the critical fluctuations are characterized by the spatial fluctuations of the order parameter. The length scale over which such fluctuations are correlated defines the correlation length,  $\xi$ , which diverges at the critical point. The order-parameter fluctuations are described in terms of a field theory, commonly called a  $\phi^4$ -theory, in  $d$  spatial dimensions.

The standard description of a QCP follows this prescription. The critical mode is still considered to be the fluctuations of the order parameter, a classical variable. The only vestige of the quantum nature of the critical fluctuations is that they take place not only in space, but also in imaginary time<sup>9,29</sup>. The correlation time,  $\tau_0$ , scales with the correlation length,  $\xi$ , defining a dynamic exponent  $z$ , via  $\tau_0 \propto \xi^z$ . For an AF metal, the result is a  $\phi^4$ -field theory, in  $d + z$  spatial dimensions, with  $z = 2$ . The finite-temperature properties of this theory have been systematically discussed<sup>10,11,30</sup>. More microscopically, an itinerant antiferromagnet is typically described in terms of a spin-density-wave state, that is, a spontaneous spatial modulation of the spins of the charge carriers, and the picture of quantum-critical order-parameter fluctuations in an itinerant antiferromagnet is also called a spin-density-wave QCP.

Theoretical studies in recent years have led to the notion that the order-parameter-fluctuation description may be insufficient, at least in some cases. Instead, inherent quantum effects play an important role<sup>12–14,31</sup>. In these cases, we need to identify the additional critical modes before a critical field theory can be constructed. The systems being considered in this context include not only HF metals, but also quantum insulating magnets. There is so far no unified framework to identify the new critical modes, and the different systems are being studied theoretically on a case-by-case basis.

In HF metals, the additional critical modes have been described in terms of the destruction of local Kondo singlets at the  $T = 0$  AF transition. In the framework of ‘local’ quantum criticality<sup>12,32</sup>, the Kondo effect is critically destroyed because local moments are coupled not only to the conduction electrons but also to the fluctuations of the other local moments. Such magnetic fluctuations, whose spectrum turns critically soft at the QCP, act as a source of dissipation and decohere the Kondo effect. This critical destruction of the Kondo effect implies that the magnetic transition is accompanied by a continuous localization–delocalization transition of the electronic excitations. A separate mechanism has been postulated in the form of spin–charge separation<sup>13</sup>. Finally, spin-liquid formation among the local moments, which may occur as a result of geometric frustration, has been proposed as a competing mechanism against Kondo-singlet formation<sup>14,33</sup>.

It is worth emphasizing the dynamical nature of the Kondo screening; see Fig. 2a. At sufficiently high temperatures, a Kondo

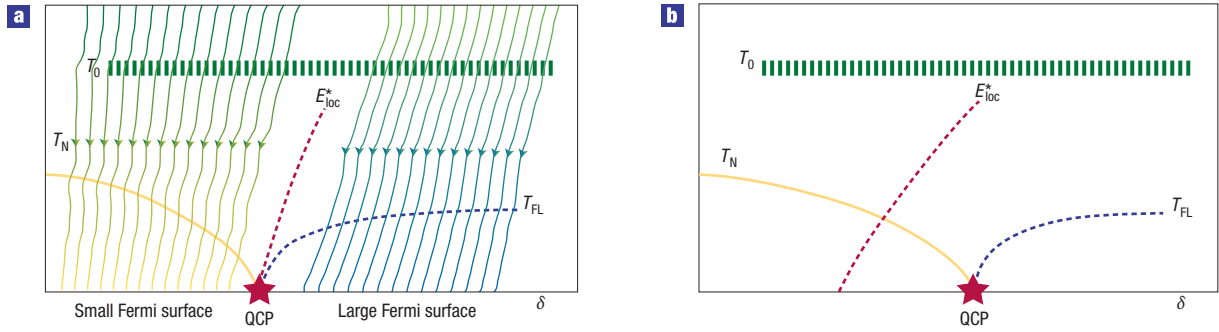


**Figure 2** Schematic phase diagrams showing two classes of QCPs. **a,b**, The temperature/energy scales versus control parameter ( $\delta$ , which tunes the ratio of the Kondo interaction to the RKKY interaction), illustrating quantum criticality with critical Kondo destruction (**a**) and of the spin-density-wave type (**b**).  $T_N$  represents the Néel temperature and  $T_{FL}$  the onset of the low-temperature FL regime. Lines with arrows correspond to renormalization-group flows, which describe the transformation of the system from the high-temperature fully incoherent regime to the zero-temperature ground states.  $E_{loc}^*$  marks an energy scale separating the renormalization-group flows towards two types of ground state—one with a large Fermi surface (Kondo resonance fully developed, and  $f$  electrons delocalized) and the other with a ‘small’ Fermi surface (static Kondo screening absent, and  $f$  electrons localized). Similar renormalization-group flows apply to **b**, but are omitted there for visual simplicity.  $T_0$  signifies the initial crossover in a Kondo lattice system, from the high-temperature regime, where the local moments are completely incoherent, to the intermediate-temperature regime, in which the initial Kondo screening operates.

lattice behaves as a collection of individual local moments, weakly coupled to a band of conduction electrons. At the temperature  $T_0$ , the initial crossover into Kondo screening sets in. We should caution that extracting  $T_0$  from the Kondo temperature of the diluted limit of a HF system is in general problematic, because the process of dilution can change the atomic volume<sup>34</sup> and other parameters. Still, the initial crossover associated with  $T_0$  of the Kondo lattice system has a similar physical meaning as that of the crossover occurring in a single-impurity Kondo problem. For definiteness, and inspired by the exact solution to the thermodynamics of the single-impurity Kondo problem<sup>35</sup>, we define  $T_0$  as twice the temperature at which the entropy is  $0.4R\ln 2$  per local moment.

Whether the Kondo screening process is complete or incomplete at sufficiently low temperatures depends on the competition between the Kondo interaction and the RKKY coupling among the moments. The line associated with the energy scale  $E_{loc}^*$  is the separation between the two regimes. On increasing  $\delta$  at a fixed temperature (Fig. 2a), the  $E_{loc}^*$  line marks the crossover from the small-Fermi-surface regime to the large-Fermi-surface one. To the right of the  $E_{loc}^*$  line the local moments are being converted into composite fermions, which are part of the Fermi volume. In this regime we find, on cooling at a fixed  $\delta$ , that FL coherence is fully established below  $T_{FL}$ . In the regime to the left of the  $E_{loc}^*$  line, the Kondo screening is incomplete even at zero temperature, and the local moments do not participate in the Fermi-surface formation. Here, the system eventually orders into an AF state below the Néel temperature,  $T_N$ ; at the lowest temperatures inside the AF phase, the system will also be a Fermi liquid (see below for further discussions). In the zero-temperature limit, the  $E_{loc}^*$  line marks a genuine  $f$ -electron-localization phase transition; at finite temperatures, it represents a crossover.

When  $E_{loc}^*$  terminates at the same value of the control parameter ( $\delta_c$ ) as the AF phase boundary (Fig. 2a), the quantum-critical fluctuations include not only the fluctuations of the magnetic order parameter but also those associated with the destruction of the Kondo effect. The local quantum-critical solution belongs to this case<sup>12,32,36–38</sup>. When the two lines intersect (Fig. 2b), the magnetic QCP falls in the category of the spin-density-wave theory. The third case, with the  $E_{loc}^*$  line terminating before meeting the

magnetic-ordering phase boundary, would imply a finite range of  $T = 0$  parameter space in which the local moments are neither Kondo screened nor magnetically ordered; this does not happen in general, although it cannot be completely ruled out if the underlying spin system is highly frustrated.

#### QUANTUM CRITICAL SCALING

Historically, scaling has played a central role in the study of classical criticality. It results from the non-analyticity in the free energy at the transition temperature  $T_c$ , and is manifested in thermodynamic properties such as specific heat and static susceptibility.

Quantum criticality shows a number of important distinctions in scaling. First, there are generically two control parameters, which are both relevant in the renormalization-group sense. One is the non-thermal control parameter,  $\delta - \delta_c$ , and the other one is the temperature  $T$ . They represent two independent directions to access the QCP ( $T = 0, \delta = \delta_c$ ) within the temperature–control-parameter phase diagram. Accessing the QCP by varying the non-thermal control parameter will lead to a divergence of the spatial correlation length,  $\xi$ . Doing so through reducing the temperature  $T$ , on the other hand, amounts to increasing the size of the temporal dimension,  $\beta = 1/k_B T$ , towards infinity. Even the scaling of thermodynamic quantities would involve judicious mixing of spatial and temporal fluctuations. This is in contrast to the case of a generic classical critical point, where the non-thermal control parameter and the reduced temperature  $(T - T_c)/T_c$  are interdependent; the variation of each will be manifested in scaling through the spatial correlation length. Second, quantum-critical scaling is also delicate owing to the very fact that a QCP exists at zero temperature. The system is therefore subject to the constraints of the third law of thermodynamics. For instance, a divergence of the specific heat often occurs at a classical critical point, but cannot occur at a QCP.

It turns out that static-scaling exponents are more conveniently defined in terms of thermodynamic ratios. A prototypical example is the Grüneisen ratio—defined<sup>39</sup> as the ratio of the volume thermal expansion to the specific heat,  $\Gamma = \beta/C_p$ . At a generic QCP where the control parameter is linearly coupled to the pressure,  $\Gamma$  must diverge, in a way that provides a thermodynamic means of

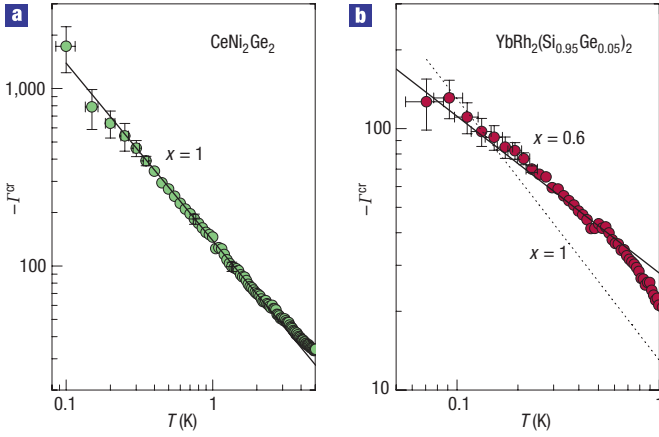


**Figure 3** Divergence of the dimensionless critical Grüneisen ratio at QCPs. **a, b**, The temperature dependence of  $\Gamma^{\text{cr}} = V_m / \kappa_T \times \beta^{\text{cr}} / C^{\text{cr}}$  for  $\text{CeNi}_2\text{Ge}_2$  (**a**) and  $\text{YbRh}_2(\text{Si}_{0.95}\text{Ge}_{0.05})_2$  (**b**), on double-log scales<sup>41</sup>. Here,  $\beta^{\text{cr}}$  and  $C^{\text{cr}}$  are the volume thermal expansion and specific heat after subtraction of normal (FL) contributions.  $V_m$  and  $\kappa_T$  are the molar volume and isothermal compressibility (at room temperature); they are used for normalization to make  $\Gamma^{\text{cr}}$  dimensionless. Error bars, standard errors. Part **a** reprinted with permission from ref. 41. © 2003 APS.

probing the universality classes<sup>39</sup>. It follows from straightforward scaling arguments that the critical Grüneisen ratio, that is, the ratio of the critical part of thermal expansion to the critical part of the specific heat, goes as  $\Gamma^{\text{cr}} \sim T^{-x}$  at the QCP. The Grüneisen exponent  $x = 1/\nu z$ , with  $\nu$  being the correlation-length exponent (via  $\xi \propto (\delta - \delta_c)^{-\nu}$ ) and  $z$  the dynamic exponent. For a magnetic-field-driven transition, a similar result applies to the magnetocaloric effect  $(1/T)\partial T/\partial H|_S$  (refs 39,40).

Divergence of the critical Grüneisen ratio has now been observed in several HF metals near their QCPs. Figure 3 shows the results for single crystals of  $\text{CeNi}_2\text{Ge}_2$  and  $\text{YbRh}_2(\text{Si}_{0.95}\text{Ge}_{0.05})_2$ . For  $\text{CeNi}_2\text{Ge}_2$ , the Grüneisen exponent  $x$  is consistent with a spin-density-wave QCP in three dimensions, which predicts  $x = 1$  (ref. 41). Similar observations have also been made for some other systems<sup>42,43</sup>. By contrast, the exponent  $x \approx 0.6$  in  $\text{YbRh}_2(\text{Si}_{0.95}\text{Ge}_{0.05})_2$  (ref. 41) cannot be explained by any spin-density-wave-QCP theory. (The exponent is roughly compatible with the ferromagnetic paramagnon picture, which, however, is not compatible with other experimental results<sup>44</sup>.) It is instead compatible with the local quantum-critical picture in the presence of  $xy$ -spin anisotropy, which has  $x \approx 0.66$  (L. Zhu, Q.S., unpublished; ref. 45). A phenomenological approach<sup>46</sup> has also yielded a fractional Grüneisen exponent  $x = 2/3$ , when an emergent spinless-fermionic field is assumed to take a certain fine-tuned dispersion; this picture, though, contains no Fermi-surface jump at the QCP. The Grüneisen exponent for  $\text{CeCu}_{6-x}\text{Ag}_x$  also deviates from the spin-density-wave prediction<sup>47</sup>.

The mixing of statics and dynamics inherent to any QCP implies that the scaling pertinent to the universality class can also be observed in dynamical measurements. A spin-density-wave QCP in three dimensions is described by a five-dimensional  $\phi^4$  field theory, which has a gaussian fixed point. The non-interacting nature of the fixed point implies that spin damping is absent at the fixed point, and that the corresponding relaxation rate must be proportional to  $T^\gamma$  with  $\gamma > 1$ ; this means that there is a violation of  $\omega/T$  scaling in the dynamical spin susceptibility<sup>2,10,11</sup>. (Here  $\omega$  is the frequency.) For any interacting fixed point, on the other hand, spin damping occurs already at the fixed-point level, and an  $\omega/T$  scaling is expected<sup>12,48,49</sup>.

In the case of  $\text{CeCu}_{5.9}\text{Au}_{0.1}$ , extensive measurements with inelastic neutron scattering have been carried out. Most surprisingly, critical scattering occurs along certain lines (as opposed to points) in  $\mathbf{q}$ -space, indicating quasi-two-dimensional (2D) quantum critical fluctuations<sup>50</sup>. However, the 2D spin-density-wave QCP picture cannot explain the observation that both at and far away from the wavevector of the nearby AF order the neutron and magnetization data show  $\omega/T$  scaling, with an anomalous exponent  $\alpha < 1$  (ref. 7). (The same exponent appears in the  $H/T$  scaling of the magnetization of  $\text{CeCu}_{5.9}\text{Au}_{0.1}$ .)

Considerable theoretical efforts have gone into understanding this scaling behaviour. Within the local quantum-critical picture, the emergent critical excitations associated with the Kondo destruction make the fixed point an interacting one, and the dynamical susceptibility shows an  $\omega/T$  scaling<sup>12,32</sup>. In the Ising-anisotropic case, appropriate for the Au-doped  $\text{CeCu}_6$  system, the fractional exponent  $\alpha$  takes a value<sup>36–38</sup> close to the experimental observation.

In  $\text{YbRh}_2(\text{Si}_{1-x}\text{Ge}_x)_2$  ( $x = 0$  and  $0.05$ ), neutron-scattering results on the critical fluctuations (as well as on the magnetic order) are not yet available. Still, a fractional exponent has been seen in the bulk linear-response susceptibility. From 10 to 0.3 K,  $\Delta\chi$  is proportional to  $T^{-0.6}$ , where  $\Delta\chi$  denotes the susceptibility after subtracting a small temperature-independent contribution<sup>51</sup>. This points to some degree of universality between  $\text{YbRh}_2\text{Si}_2$  and  $\text{CeCu}_{5.9}\text{Au}_{0.1}$ . At the same time, there also exist some important differences between these two systems. The bulk susceptibility of  $\text{YbRh}_2(\text{Si}_{1-x}\text{Ge}_x)_2$  is very strongly enhanced at low temperatures. Related behaviour is also found in the field dependence of the ( $T \rightarrow 0$ ) Pauli susceptibility  $\chi_0$  above the critical field  $H_c$ . In addition, the Sommerfeld–Wilson ratio of  $\chi_0$  to the electronic specific heat coefficient,  $\gamma = C_d/T$ , is extremely enhanced compared with usual HF metals and exceeds a value of 30 on approaching the critical field<sup>51</sup>. These observations have been described in terms of a very small Weiss field at  $\mathbf{q} = \mathbf{0}$  (ref. 44). A recent proposal<sup>52</sup> associates the enhanced ferromagnetic fluctuations with a possible nearby quantum tricritical point. Enhanced ferromagnetic correlations might be responsible for the sharp  $\text{Yb}^{3+}$  ESR line observed well below  $T_0$  (ref. 53).

The issue of violation of  $\omega/T$  scaling in candidate spin-density-wave QCPs has not yet been extensively studied. As will be discussed later, some indication in this direction has appeared in lightly Rh-doped  $\text{CeRu}_2\text{Si}_2$  (ref. 54).

## DIVERGENCE OF EFFECTIVE MASS

A key characteristic of both  $\text{CeCu}_{5.9}\text{Au}_{0.1}$  and  $\text{YbRh}_2\text{Si}_2$  is the divergence of the effective charge-carrier mass at the QCP. The case of  $\text{YbRh}_2\text{Si}_2$  is illustrated in Fig. 4. The magnetic field tunes the system through a QCP at  $H_c$ , as reflected in the evolution of the specific heat and electrical resistivity. Between 10 and 0.3 K, the electronic specific-heat coefficient  $\gamma$  shows a logarithmic divergence. A similar logarithmic divergence was also seen in  $\text{CeCu}_{5.9}\text{Au}_{0.1}$ . A feature that has been observed in  $\text{YbRh}_2\text{Si}_2$ , but not in  $\text{CeCu}_{5.9}\text{Au}_{0.1}$ , is the more singular  $T^{-0.4}$  dependence found below 0.3 K. For  $H > H_c$ , both the specific heat and the electrical resistivity of 5-at.%-Ge-doped  $\text{YbRh}_2\text{Si}_2$  show scaling over almost four decades in  $(H - H_c)/T$  (ref. 55). Within the FL regime,  $\gamma \propto (H - H_c)^{-1/3}$ . FL theory enables us to identify the value of  $\gamma$  at zero temperature with the effective mass of Landau quasiparticles, appropriately averaged over the Fermi surface. Hence, the latter can be inferred to diverge as the QCP is reached.

For  $\text{CeNi}_2\text{Ge}_2$  (ref. 41) and  $\text{CeCu}_2\text{Si}_2$  (ref. 56), by contrast, the effective mass seems to be finite. (For both compounds, low-temperature upturns are observed in the normal-state

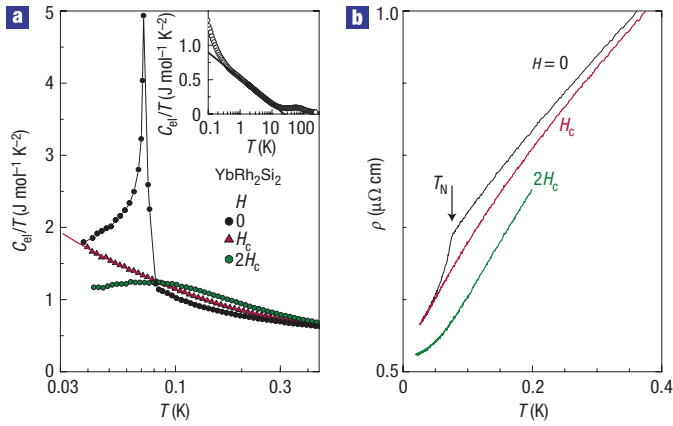


**Figure 4** Thermodynamic and transport properties close to the QCP in  $\text{YbRh}_2\text{Si}_2$ . **a**, Low-temperature electronic specific-heat coefficient at various different fields applied perpendicular to the  $c$ -axis<sup>124</sup>. At the critical field,  $H_c \approx 0.055$  T, the specific-heat coefficient goes as  $T^{-0.4}$  at low temperatures and as  $-\ln T$  at higher temperatures. Inset: The zero-field data over an extended temperature range, illustrating the onset of the  $\ln T_0/T$  dependence at  $T \approx 10$  K ( $T_0 = 24$  K) and the onset of a power-law divergence at  $T \approx 0.3$  K (ref. 8). **b**, Low-temperature electrical resistivity<sup>125</sup> as a function of temperature at the same magnetic fields as in **a**.

$C_{el}/T$  results. These upturns are very likely not part of the quantum criticality<sup>41</sup>.)

A divergent effective mass naturally arises on approach to a Kondo-destroying QCP, because a critical destruction of Kondo screening leads to the vanishing of quasiparticle weight everywhere on the Fermi surface. In a spin-density-wave QCP, the vanishing of quasiparticle spectral weight occurs only near the ‘hot spots’, the portions of the Fermi surface that are connected by the AF wavevector. On all other parts of the Fermi surface, kinematic constraints prevent the overdamped spin fluctuations from scattering the electrons; the quasiparticles are well defined, with a finite mass. (This anisotropy is also manifested in the electron scattering rates, which have the NFL and FL forms at the hot spots and cold regions, respectively. In the clean limit, the current carried by cold electrons short-circuits that carried by the hot electrons, making  $\Delta\rho \propto T^2$  even above  $T_{FL}$  on cooling near the QCP<sup>57,58</sup>.) For a three-dimensional (3D) spin-density-wave QCP, the Fermi-surface-averaged effective mass appearing in the specific-heat coefficient is finite.

As alluded to in the introduction, the entropy associated with the scaling regime is very large—about  $0.4R \ln 2$  per Yb moment<sup>8</sup>. It is truly striking that quantum-critical excitations accumulate nearly half of the full entropy associated with the atomic physics of the lowest doublet of each  $\text{Yb}^{3+}$  ion. This result exemplifies how quantum criticality is able to reach up in temperature and influence a large part of the phase diagram of strongly correlated electron systems<sup>59</sup>.

## FERMI SURFACE AND ENERGY SCALES

### COLLAPSE OF FERMI SURFACE

The evolution of the Hall effect across the QCP has been studied in ref. 60 for  $\text{YbRh}_2\text{Si}_2$ . The linear-response Hall coefficient, as shown in Fig. 5a, shows a broadened step when the system is tuned (with the field applied in the magnetic easy plane parallel to the current direction) across the QCP. This feature sharpens on decreasing the temperature, extrapolating to a jump in the zero-temperature limit, precisely at the QCP.

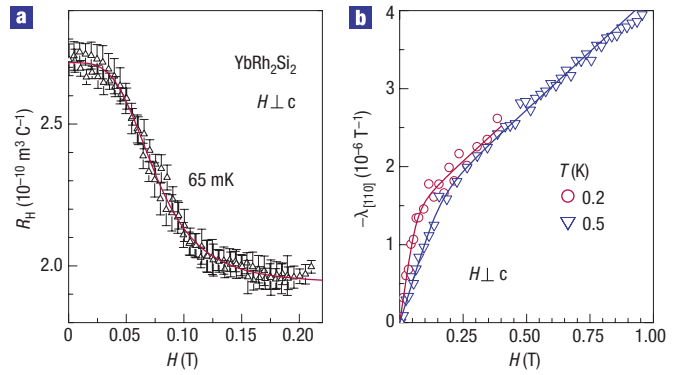


**Figure 5** Evidence for an additional low-energy scale in the Hall-effect and thermodynamic data of  $\text{YbRh}_2\text{Si}_2$ . **a**, Linear-response Hall coefficient  $R_H$  as derived from the initial slope of the Hall resistivity in a crossed-field experiment<sup>126</sup>, carried out on the same single crystal as used in ref. 60. Error bars, standard errors. The crossover width decreases with temperature, extrapolating to zero in the zero-temperature limit<sup>60</sup>. **b**, Magnetic-field dependence of the magnetostriction of a high-quality single crystal ( $\rho_0 \approx 0.5 \mu\Omega \text{ cm}$ ). The symbols represent the linear coefficient  $\lambda_{[110]} = \partial \ln L / \partial H$  (where  $L$  is the sample length along the  $[110]$  direction within the tetragonal  $ab$  plane) versus  $H$  at different temperatures<sup>44</sup>.

For a spin-density-wave QCP, the system orders into a spin-density-wave state, which breaks translational invariance. This order generically removes the hot spots of the Fermi surface, and leads to a reconstruction of the Fermi surface. Still, the gradual onset of the spin-density-wave order implies a smooth evolution of the Fermi surface, and the Hall coefficient is continuous across the QCP<sup>13,61</sup>. Precisely this type of evolution has been seen in the Hall coefficient of V-doped Cr (ref. 62), which is considered a prototypical system for a spin-density-wave quantum phase transition.

The Hall data in  $\text{YbRh}_2\text{Si}_2$ , by contrast, suggest a sudden change of the Fermi surface at the QCP<sup>60</sup>. The extrapolated zero-temperature jump, being inconsistent with the spin-density-wave QCP picture, is naturally interpreted in terms of a collapse of the large Fermi surface: it is as if a large number of charge carriers of the non-magnetic phase are suddenly lost as we tune the system through the QCP. As can be seen from Fig. 2, this is precisely what happens in a Kondo-destroying QCP: the destruction of Kondo resonances at the magnetic QCP converts the large Fermi surface of the paramagnetic HF metal into a small one.

A traditional means to measure the Fermi surface is the de Haas-van Alphen (dHvA) technique. Recent dHvA experiments<sup>63</sup> have detected a sudden change of the Fermi surface as a function of pressure in the field-induced normal state of  $\text{CeRhIn}_5$  (see Fig. 8 below). As we will discuss shortly, it is possible that the threshold pressure seen in the dHvA measurement on  $\text{CeRhIn}_5$  corresponds to an AF QCP<sup>64</sup>.

### MULTIPLE ENERGY SCALES

The Fermi surface is sharply defined only at zero temperature. Figure 2 naturally suggests that the contrast between the two types of QCP should also be manifest in the energy scales of the equilibrium many-body excitation spectrum and, hence, in the finite-temperature properties as well. For the spin-density-wave QCP, the critical modes correspond to the slow fluctuations of the magnetic order parameter. Dynamical scaling implies that their energy scale vanishes at the approach to the QCP. For the Kondo-destroying QCP, the critical Kondo effect specifies inherently

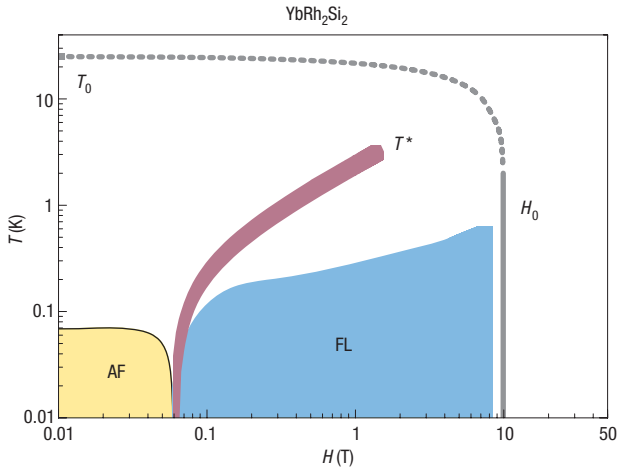


**Figure 6** The temperature-versus-magnetic-field phase diagram for  $\text{YbRh}_2\text{Si}_2$ . The magnetic field ( $H$ ) is applied perpendicular to the crystallographic  $c$ -axis. Dashed and solid grey lines show the initial Kondo crossover scale  $T_0 = 25$  K (at  $H = 0$ ) and the corresponding  $H_0$ , which suppresses the heavy quasiparticle behaviour<sup>27</sup>. The fine black line indicates the boundary of the AF phase<sup>87</sup>. The broad red line specifies the position of crossover in the isothermal Hall resistivity<sup>60</sup>, which agrees with that observed in the isothermal magnetostriction, magnetization and longitudinal resistivity<sup>44</sup> and marks an additional low-energy scale. The regime at  $H > H_c$ , where the electrical resistivity follows the Landau FL behaviour  $\Delta\rho \propto T^2$ , is shown in blue<sup>87</sup>. A double-log representation has been used for clarity.

quantum-mechanical excitations that are in addition to critical fluctuations of the order parameter. We can therefore expect the occurrence of more than one energy scale, all of which vanish as the QCP is reached. The Hall-effect measurement in  $\text{YbRh}_2\text{Si}_2$ , described earlier, had in fact proven the existence of a  $T^*(H)$  line (Fig. 6) (ref. 60).

The Hall-effect crossover is accompanied by changes in the slope of the isothermal magnetization and magnetostriction<sup>44</sup>. As shown in Fig. 5b, the latter shows a kink-like structure whose position in field matches the position of the Hall-effect crossover. This proves that the low-energy scale  $T^*(H)$  is intrinsic to the equilibrium excitation spectrum. The energy scale is separate from both the Néel temperature and  $T_{\text{FL}}$ , the boundary of the FL regime (Fig. 6). The distinction between  $T^*$  and  $T_{\text{FL}}$  is reinforced by the differences in how the physical properties behave<sup>44</sup>: various isothermal properties show a temperature-smearred jump across the  $T^*$  line, but are always smooth across the  $T_{\text{FL}}$  line. In the  $T \rightarrow 0$  limit, the lines defined by the three energy scales merge at the same point, the field-induced<sup>44,60</sup> QCP.

The comparison between the thermodynamic results with the Hall-effect data suggests that  $T^*(H)$  is the finite- $T$  manifestation of the localization of the  $f$  electrons at the QCP. This in turn suggests that the measured  $T^*(H)$  scale characterizes the Fermi-surface collapse at zero temperature<sup>44,60</sup>. It corresponds to the  $E_{\text{loc}}^*$  scale of the local quantum-critical picture<sup>12</sup>, shown in Fig. 2a. Multiple vanishing energy scales also arise in the ‘deconfined’ quantum-criticality scenario for insulating quantum magnets<sup>31</sup>; in its extension to itinerant HF systems<sup>14,65</sup>, though, the additional energy scale vanishes at a point away from the magnetic QCP.

It is instructive to contrast the case of  $\text{YbRh}_2\text{Si}_2$  with what happens in the V-doped Cr. There, the changes in the Hall coefficient occur only at the Néel transition<sup>62,66</sup>. By extension, there is no indication for a separate  $T^*$  scale<sup>60</sup>. These observations

are consistent with the spin-density-wave QCP description of V-doped Cr.

The hexagonal compound  $\text{YbAgGe}$  is another Yb-based HF system that undergoes field-induced magnetic quantum phase transitions<sup>67</sup>. It shares some similarities with  $\text{YbRh}_2\text{Si}_2$ . In particular, Hall-effect measurements in this material have also shown an anomaly that defines a crossover line in the temperature-versus-field phase diagram<sup>68</sup>. Unlike the case for  $\text{YbRh}_2\text{Si}_2$ , however, the features associated with the ‘Hall line’ have not yet allowed a linkage with a Fermi-surface jump in the zero-temperature limit. There are also some other important differences between the two systems. Compared with  $\text{YbRh}_2\text{Si}_2$ ,  $T_N$  in  $\text{YbAgGe}$  at ambient pressure is much larger (about 1 K) and, correspondingly, the critical field is much greater (about 5 T). The temperature versus field phase diagram is considerably more complex, with additional first-order transitions inside the AF region and a metamagnetic signature in  $M(H)$  when crossing the Hall line<sup>69</sup>. Thermodynamic and transport measurements in  $\text{YbAgGe}$  have raised the possibility that an NFL phase occurs over an extended range of magnetic fields<sup>67</sup>. Given the hexagonal crystal structure, the underlying spin system may very well be frustrated; it is hence natural to raise the question about the potential role that geometrical frustration plays in influencing the phase diagram of  $\text{YbAgGe}$ .

## SUPERCONDUCTIVITY

In the past few years growing evidence has been collected for more than one non-phononic pairing mechanism operating in different HF superconductors. These include Cooper pairing possibly mediated by nearly critical valence fluctuations<sup>70</sup> in both  $\text{CeCu}_2\text{Ge}_2$  (ref. 71) and  $\text{CeCu}_2\text{Si}_2$  (ref. 72) under high pressure (Fig. 7), by AF magnons in  $\text{UPd}_3\text{Al}_3$  (ref. 73) and ferromagnetic ones in pressurized  $\text{UGe}_2$  (ref. 74) as well as  $\text{URhGe}$  (ref. 75) and  $\text{UCoGe}$  (ref. 76).

$\text{CeCu}_2\text{Si}_2$  (at ambient and low pressure) is the prime candidate for antiparamagnon-mediated superconductivity near a 3D spin-density-wave QCP<sup>72</sup>. This is illustrated in Fig. 7, where a low-pressure dome of superconductivity occurs near the AF QCP for 10-at.%-Ge-doped  $\text{CeCu}_2\text{Si}_2$ . From neutron-diffraction measurements on an AF (‘A-type’) single crystal<sup>77</sup>, the latter was found to be of the spin-density-wave variety. In addition, the  $\Delta\rho \propto T^{1.5}$  and  $\gamma(T) = \gamma_0 - \alpha T^{0.5}$  dependencies found earlier in the low-temperature normal state in ‘S-type’ samples located on the strong-coupling side of the QCP<sup>56</sup> suggested that the correlated critical fluctuations are 3D. Ongoing inelastic-neutron-scattering experiments carried out on ‘S-type’  $\text{CeCu}_2\text{Si}_2$  single crystals<sup>78</sup> are devoted to searching for quantum-critical spin-density-wave fluctuations, which were proposed to act as superconducting glue in this case<sup>79,80</sup>. Future neutron-diffraction experiments on other NFL superconductors like  $\text{CePd}_2\text{Si}_2$  (ref. 79) are urgently needed to gain more insight into the relationship between quantum criticality and superconductivity.

The available results, however, highlight a surprisingly rich diversity in physical scenarios. For instance, superconductivity may occur from the proximity to a field-induced QCP, as in  $\text{CeCoIn}_5$  (ref. 81) and perhaps also in  $\text{UBe}_{13}$  (ref. 82).

Microscopic theories of HF superconductivity were mostly constructed before the period of active studies on quantum criticality. Given that a large number of HF superconductors are now recognized as being close to a QCP, it is important that the interplay between quantum criticality and superconductivity be systematically studied in the future. More generally, it is likely that HF superconductors will have an important role to play in the larger understanding of strongly correlated superconductors<sup>83</sup>.

## DISCUSSION

The subject of quantum-critical HF metals is a vast one and the present article, not meant to be comprehensive, is unable to cover all the interesting topics. We now touch on some of these, in the hope of pointing the practitioners to—and providing the uninitiated readers with a glimpse of—some issues that are worthy of further exploration.

### QUANTUM PHASES VIS-A-VIS QCPS

The different types of magnetic QCP, illustrated in Fig. 2, suggest that the magnetic quantum phases also come in different classes. The presence or absence of Kondo screening, which influences quantum criticality, also leads to distinct Fermi surfaces in a magnetically ordered HF metal. The issue is of larger importance: the need to use the Fermi surface to distinguish between various zero-temperature magnetic phases implies the failure of the Landau assumption that an order parameter alone characterizes quantum phases.

The Kondo screening deep inside the AF part of the Kondo-lattice phase diagram was studied recently<sup>84,85</sup>. The Kondo interaction is shown to be exactly marginal in the renormalization group sense (with respect to the zero-Kondo-coupling fixed point). The result provides a firm theoretical basis for the existence of an AF metal with a small Fermi surface—an AF<sub>S</sub> phase in which the local moments (behaving as localized core electrons) do not participate in the formation of the electronic Fermi volume. This phase is different from the AF<sub>L</sub> phase, in which the Fermi surface is large in the sense that the local moments are part of the electronic fluid. Note that, because the AF ordering breaks the lattice translational symmetry, the Brillouin zone in a commensurate antiferromagnet is half that of the paramagnetic state. When counted in the magnetic Brillouin zone, the distinction between the AF<sub>S</sub> and AF<sub>L</sub> phases does not lie in the Fermi volume, but in the Fermi-surface topology. The two phases are separated by a Lifshitz transition. The same applies to incommensurate antiferromagnets, to linear order in the magnetic order parameter. Note also that the AF<sub>S</sub> and AF<sub>L</sub> phases may share the same magnetic structure; the main distinction between the two occurs in the electronic excitations, that is, in the nature of the Fermi surfaces.

In the paramagnetic phase, on the other hand, the Kondo interaction is traditionally understood to be relevant in the renormalization group sense<sup>23</sup>. The strong-coupling nature of the fixed point signifies that the local moments and spins of the conduction electrons form a (Kondo) singlet ground state. As described in the first section, the Kondo resonances develop and the Fermi surface is large in this paramagnetic metal phase (PM<sub>L</sub>) (ref. 23).

There has been a long history of experimental studies of the Fermi surface at low temperatures by probing dHvA oscillations (for a recent review, see ref. 86). Measurements in the antiferromagnetically ordered HF metals have provided extensive evidence for the AF<sub>S</sub> phase; a typical example is CeRh<sub>2</sub>Si<sub>2</sub>, which is antiferromagnetically ordered at ambient pressure. In paramagnetic HF metals, evidence for the PM<sub>L</sub> phase has existed since the early days of HF studies.

One intriguing aspect with the AF<sub>S</sub> phase concerns the quasiparticle mass. Mass enhancement in HF metals is traditionally associated with the Kondo resonances, as is appropriate for both the PM<sub>L</sub> and AF<sub>L</sub> phases. How can a large mass arise in the AF<sub>S</sub> phase? To see this, it is important to recognize that the Kondo destruction in the AF<sub>S</sub> phase refers to the vanishing of the static amplitude of the Kondo singlet. The small Fermi surface is a property of the ground state; in other words, the discontinuity in the ground-state momentum distribution occurs at the small Fermi surface, and

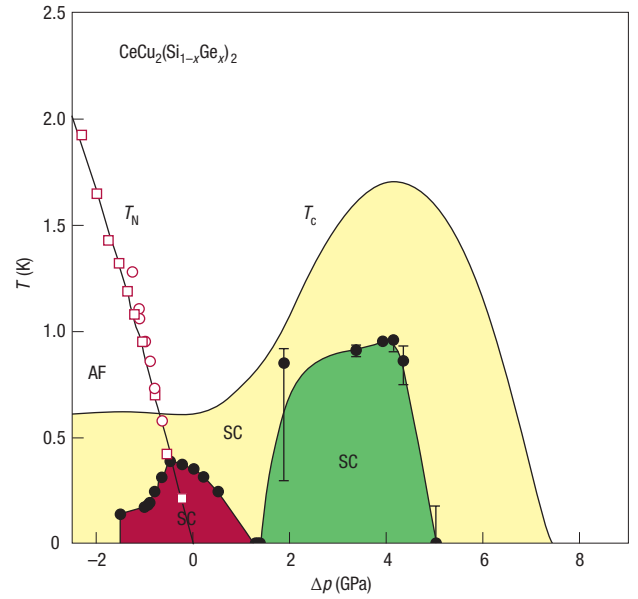


**Figure 7** Pressure dependence of magnetic order and superconductivity in  $\text{CeCu}_2(\text{Si}_{1-x}\text{Ge}_x)_2$ . Transition temperatures for Néel ordering ( $T_N$ ) and superconductivity ( $T_c$ ) are shown as a function of pressure increment  $\Delta p = p - p_{c1}$ . Error bars represent the width of superconducting transitions in the electrical resistivity. For  $T_N$  the open circles (squares) correspond to  $x = 0.1$  ( $x = 0.25$ ), and for  $T_c$  the thin solid line (full circles) is for  $x = 0$  ( $x = 0.1$ ). The reference pressure  $p_{c1}$  is 0.4 GPa (for  $x = 0$ ), 1.5 GPa ( $x = 0.1$ ), 2.4 GPa ( $x = 0.25$ ) and 11.5 GPa ( $x = 1$ ) (ref. 72).

not where the large Fermi surface would be located. The effective mass, on the other hand, is a dynamical quantity; it measures the dispersion of single-electron excitations, that is, quasiparticles. The effective mass in the AF<sub>S</sub> phase is enhanced owing to the dynamical part of the Kondo-singlet correlations. That dynamical Kondo correlations should persist in the AF<sub>S</sub> phase is intuitively clear. This has been demonstrated in some dynamical studies of the magnetically ordered region of the Kondo lattice model<sup>36–38</sup>, and is also in part reflected in the marginal nature of the Kondo coupling in the renormalization-group study mentioned earlier<sup>84,85</sup>.

The mass enhancement in the AF<sub>S</sub> phase is also important for the Kondo-destroying QCP. Because the effective mass diverges as the QCP is approached from the paramagnetic side, continuity dictates the same to be true as the QCP is approached from the magnetically ordered side. Experimentally, a large effective mass has been observed in the ordered states of both  $\text{CeCu}_{6-x}\text{Au}_x$  and  $\text{YbRh}_2\text{Si}_2$  (refs 6,87).

We close this subsection by addressing the theoretical studies of the destruction of the Kondo effect within single-impurity Kondo-type problems. These works complement the studies already mentioned in the case of Kondo lattice systems; through extended dynamical mean-field studies, for instance, these works have had considerable cross-talk with those on the lattice problem. The physics of the critical Kondo-destruction effect and the associated scaling properties have been most extensively studied within the Bose–Fermi Kondo model<sup>88–92</sup>. A related Kondo-destruction effect has also been studied in a single-impurity Kondo problem whose conduction-electron host is placed near its spin-density-wave QCP<sup>93</sup>. Finally, the formulation of the single-impurity Kondo problem in a Schwinger-boson representation<sup>94</sup>, although not directly concerned with the Kondo-destruction effect, holds the promise to handle magnetism

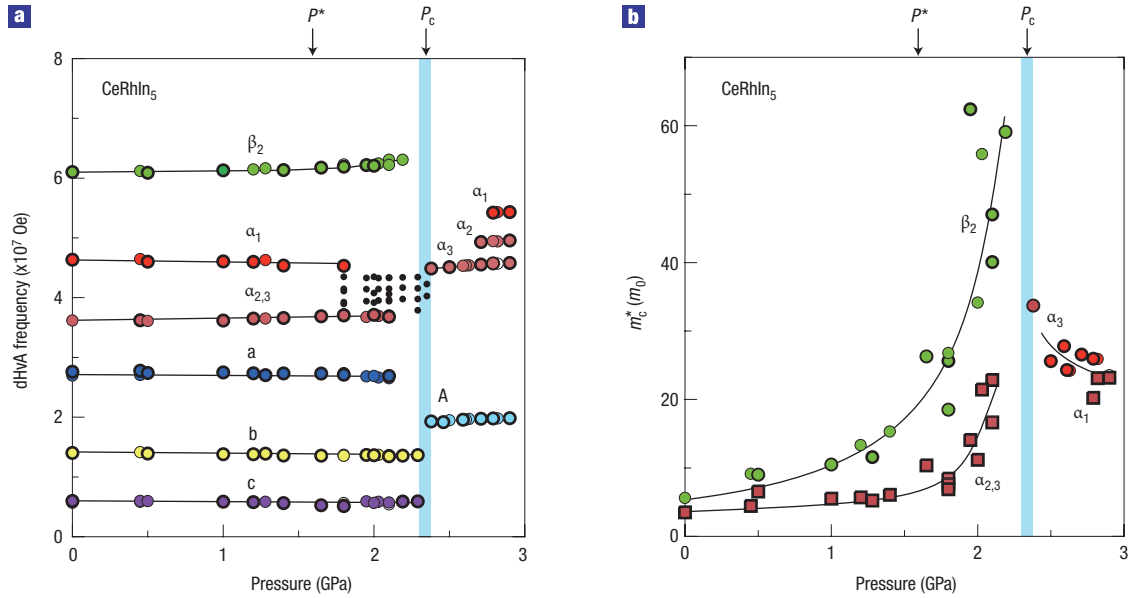


**Figure 8** Changes of Fermi surface properties across a likely QCP in CeRhIn<sub>5</sub>. **a,b**, The pressure dependence of the dHvA frequencies (**a**) and cyclotron mass<sup>63</sup> (**b**).

and the Kondo effect of the Kondo-lattice problem within a large- $N$  treatment.

#### OTHER POTENTIALLY QUANTUM-CRITICAL HF METALS

From the materials perspective, the quantum-critical HF metals we have most extensively discussed so far (Fig. 1) are distinct in that the existence of a QCP has been established explicitly: AF order has been observed and, moreover, has been continuously suppressed to  $T = 0$ . There is a sizable number of other HF metals in which QCPs have been implicated.

One case is CeRhIn<sub>5</sub>, whose low-temperature phase diagram is gradually being uncovered. It is an antiferromagnet at ambient pressure and turns into a superconductor when the applied pressure is sufficiently large. Applying a magnetic field inside the superconducting region induces a smooth transition between a purely superconducting phase and one in which superconductivity and antiferromagnetism coexist<sup>64,95</sup>. A particularly exciting possibility occurs at a magnetic field of more than 9 T, where applying pressure induces a direct second-order transition from a purely AF phase to a non-magnetic one. This has been hinted at through an extrapolation of the lower-field measurements of ref. 64. However, direct thermodynamic/transport/neutron-scattering measurements are not yet available.

Establishing such a high-field, high-pressure AF QCP is especially important in light of the existing dHvA results<sup>63</sup>, which were obtained in magnetic fields of the order of 10 T. Figure 8 illustrates the potential jump of the Fermi volume, and divergence of the cyclotron mass, at a pressure coinciding with the critical pressure  $p_c \approx 2.3$  GPa for the putative QCP (see, however, our discussion on CeRu<sub>2</sub>Si<sub>2</sub> below). These observations imply that, if the underlying physics is indeed a second-order AF quantum phase transition, the quantum criticality would be of the Kondo-destroying type. By extension, it could be that the nearby superconductivity is promoted by unconventional quantum criticality.

The situation in CeCoIn<sub>5</sub> is more complex. There have been extensive measurements that have implicated an AF QCP at<sup>96,97</sup>

or slightly below<sup>98</sup> the upper critical field for superconductivity. Results of thermal expansion measurements on CeCoIn<sub>5</sub>, made as a function of temperature at magnetic fields slightly larger than  $H_{c2}(0)$ , suggest a crossover from 2D to 3D quantum critical spin-density-wave fluctuations when the sample is cooled to below  $T \approx 0.3$  K (ref. 99). Although long-range AF order has not yet been observed in the pure compound, it was recently identified in CeCoIn<sub>5</sub> moderately doped with Cd (ref. 100). It will be important to establish whether the AF order can be continuously suppressed as a function of Cd doping, perhaps in high magnetic fields.

Pronounced NFL behaviour in thermodynamic and transport properties has also been found in the normal state of the actinide HF superconductor UBe<sub>13</sub> and tentatively been ascribed to a field-induced AF QCP covered by the superconducting state<sup>82</sup>.

CeNi<sub>2</sub>Ge<sub>2</sub> is a prototypical HF metal showing NFL phenomena in accord with a 3D spin-density-wave QCP scenario<sup>41</sup>. Under increasing magnetic field, the crossover temperature from the NFL regime to the Landau FL one was found to continuously increase<sup>101</sup>. As in the case of CeCoIn<sub>5</sub>, AF order does not occur in the pure CeNi<sub>2</sub>Ge<sub>2</sub> but has been seen when Ni is substituted by, for example, Cu (ref. 102).

In cubic CeIn<sub>3</sub>, AF order ( $T_N \approx 10$  K) can be continuously suppressed by substituting Sn for In. The data are consistent with a QCP of the 3D spin-density-wave type at  $x_c \approx 0.67$  and a low-temperature Landau FL phase at  $x > x_c$  (ref. 42). The extent to which disorder influences the quantum-critical properties of this material remains to be clarified.

Inelastic-neutron-scattering studies have played a vital role in our understanding of quantum criticality in HF metals. Indeed,  $\omega/T$  scaling in the inelastic-neutron-scattering spectrum was observed very early on, in the Pd-doped UCu<sub>5</sub> system<sup>49</sup>, and was subsequently studied in the Au-doped CeCu<sub>6</sub> system<sup>7,50</sup>. Single crystals of the HF system Ce(Ru<sub>1-x</sub>Rh<sub>x</sub>)<sub>2</sub>Si<sub>2</sub> show an AF ordering for relatively small  $x$ . The thermodynamic or transport data are consistent with a magnetic QCP at  $x_c \approx 0.04$ , although the phase boundary has not been followed to low enough temperatures (below 3 K). Near  $x_c$ , the inelastic-neutron-scattering data<sup>54</sup> are well described by the form  $\chi(\mathbf{q}, \omega) = \chi_q(T)/[1 - i\omega/\Gamma_q(T)]$ ;

at the AF wavevector  $\mathbf{Q}$ ,  $\Gamma_Q$  has a temperature dependence of  $T^{3/2}$ . The violation of  $\omega/T$  scaling occurs in a way that it is consistent with the 3D spin-density-wave QCP<sup>9–11</sup>. The magnetic fluctuations are 3D<sup>54</sup>, in contrast to the quasi-2D behaviour<sup>7,50</sup> seen in  $\text{CeCu}_{6-x}\text{Au}_x$ . Separately, neutron-scattering results on  $\text{Ce}_{1-x}\text{La}_x\text{Ru}_2\text{Si}_2$  indicate that it shows a 3D spin-density-wave QCP with a critical concentration  $x_c \approx 0.075$  (ref. 103). Those on  $\text{Ce}(\text{Ru}_{1-x}\text{Fe}_x)_2\text{Ge}_2$  have revealed some complex dynamical scaling behaviour around  $x_c \approx 0.77$  (ref. 104).

#### GENERALITY OF MULTIPLE ENERGY SCALES

The transport and thermodynamic measurements of the multiple energy scales have considerably clarified the quantum criticality in  $\text{YbRh}_2\text{Si}_2$ . It is natural to ask about the extent to which the multiple energy scales characterize other HF metals near their QCPs.

As described earlier, the quantum-critical properties of Au-doped  $\text{CeCu}_6$  share many similarities with those of  $\text{YbRh}_2\text{Si}_2$ . Together, the two materials represent the clearest candidates for Kondo-destroying quantum criticality. It will be important to determine whether a  $T^*$  line meeting the  $T_N$  and  $T_{FL}$  lines in the zero-temperature limit (Fig. 6, for  $\text{YbRh}_2\text{Si}_2$ ) also occurs in  $\text{CeCu}_{6-x}\text{Au}_x$ . At  $x = x_c = 0.1$ , this can be done simply by studying the isothermal field dependence of various thermodynamic and transport properties.

At  $x > x_c$ , such studies can clarify the interesting contrast between the pressure-induced and magnetic-field-induced QCPs. The pressure-induced QCP at  $x > x_c$  shares the properties of the QCP in the  $x = x_c$  compound at ambient pressure<sup>5</sup>. The field-induced QCP at  $x > x_c$ , on the other hand, behaves very differently. Such a field-induced QCP was first realized in the system  $\text{CeCu}_{6-x}\text{Ag}_x$  ( $x_c \approx 0.8$ ), with indications for a field-induced 3D spin-density-wave QCP<sup>105</sup>; this behaviour is in sharp contrast to the zero-field quantum-critical behaviour observed in  $\text{CeCu}_{5.9}\text{Au}_{0.1}$  (refs 7,50). The inelastic-neutron-scattering results at the field-induced QCP in  $\text{CeCu}_{5.8}\text{Au}_{0.2}$  are also compatible with a QCP of the 3D spin-density-wave type<sup>106</sup>. Theoretical understanding of this contrast between the pressure- and field-induced QCPs is not yet available. Studying the  $T^*$  crossover line should provide new insights into this and related issues.

Even in the case of  $\text{YbRh}_2\text{Si}_2$ , it will be important to understand how the relationship between the  $T^*$ ,  $T_N$  and  $T_{FL}$  lines evolves when the strength of magnetic ordering is modified, either by Co and Ir doping<sup>107</sup> or by applying pressure<sup>8</sup>.

We have also mentioned a number of candidate HF metals in which the QCPs may be of the 3D spin-density-wave type, in particular  $\text{CeCu}_2\text{Si}_2$ . These cases also lead to several interesting questions. As suggested by Fig. 2b, the  $T^*$  crossover line can in principle be located not too far away from the magnetic QCP. Moreover, as discussed above, in the zero-temperature limit, Fig. 2b implies a Lifshitz transition within the AF part of the phase diagram. Its existence will also have to be checked for experimentally.

#### HF METALS VERSUS WEAK ITINERANT ANTIFERROMAGNETS

Our focus in this article has been on the AF HF metals. The Kondo phenomenon is central to the HF physics *per se*. Moreover, because the Kondo effect involves quantum entanglement, critical Kondo destruction naturally introduces inherently quantum excitations that are beyond those associated with the slow fluctuations of the AF order parameter.

Given this emphasis on the Kondo phenomenon, it will be important to compare and contrast the quantum criticality of AF HF metals with that of transition-metal-based weak itinerant antiferromagnets. In the latter systems, the Kondo effect is not expected to play any role (because, here, the  $d$  electrons are

itinerant—in contrast to the localized  $f$  electrons), and it would be more natural to apply the spin-density-wave QCP picture. Unfortunately, the situation is not so straightforward. There are issues both experimentally and theoretically.

Experimentally, a prototype example for a second-order quantum phase transition in weak itinerant antiferromagnets is V-doped Cr. We have already mentioned the signatures of the magnetic quantum phase transition in Hall-coefficient measurements. Transport and thermodynamic experiments, however, have failed to see any signature of the NFL excitations. Presumably, the reason has to do with the relative weakness of the electron–electron interactions, which makes the amplitude of the NFL parts in, for example, the electrical resistivity and specific heat relatively small. Better candidate materials to study the NFL excitations in the quantum-critical regime of weak itinerant antiferromagnets will probably come from transition-metal-based intermetallic compounds.

Very recently, a logarithmic divergence of the low-temperature specific heat coefficient and a  $\Delta\rho \propto T^{1.5}$  dependence in the electrical resistivity has been observed in a slightly Nb-rich single crystal of the  $d$ -electron system  $\text{NbFe}_2$  (ref. 108). In this case, the fluctuation spectrum may be complicated because strong ferromagnetic fluctuations seem to be present close to the disappearance of a (possibly long-wavelength) spin-density-wave phase.

From a theoretical perspective, even though the Kondo effect is absent, these systems still contain gapless electronic excitations. Studies by various groups have shown that in the process of integrating out such gapless electronic excitations and constructing an effective theory for the order-parameter fluctuations, non-analyticity develops in the coupling constants for the latter, which may in turn change the form of the quantum criticality<sup>109,110</sup>.

#### THE CASE OF FERROMAGNETIC QUANTUM CRITICALITY

Ferromagnetic quantum phase transitions have hardly been studied in HF metals. Ferromagnetic ordering in HF metals is rare to begin with, compared with AF ordering. What is more, in cases in which the Curie temperature can be tuned, other instabilities—such as those leading to AF phases—typically occur when the Curie temperature is sufficiently reduced<sup>111,112</sup>.

In the weak itinerant ferromagnets<sup>113</sup> such as  $\text{MnSi}$  (ref. 114),  $\text{ZrZn}_2$  (ref. 115) and  $\text{FeGe}$  (ref. 116), the transition becomes first order when the Curie temperature is sufficiently reduced. (More precisely,  $\text{MnSi}$  shows a spiral magnetic ordering with a long spiral pitch.) One of the outstanding questions is why NFL behaviour still occurs even though the quantum phase transition itself is of first order. In fact, in  $\text{MnSi}$ , the NFL behaviour in the electrical resistivity occurs in such a wide pressure range (from the critical pressure  $p_c$  up to at least  $2p_c$ )<sup>114</sup> that it may very well be the property of an NFL phase, as opposed to being associated with the fluctuations of any QCP.

Theoretically, the non-analyticities associated with integrating out the gapless conduction electrons of the weak itinerant ferromagnets provide a generic mechanism for the first-order nature of the ferromagnetic quantum phase transitions<sup>109</sup>. In the presence of Ising anisotropy, however, such non-analyticity effects should not occur<sup>109</sup>, and the corresponding quantum criticality is supposed to be of the order-parameter-fluctuation type. This makes it particularly appealing to study quantum criticality in metamagnetic systems.

A metamagnetic transition describes the sudden onset of the magnetization as a function of magnetic field. This transition involves two phases of the same symmetry. Being in the same class as the melting transition of ice to water, it is of first order. A line of first order transitions in this case will terminate

at a critical end point. By tuning one additional parameter, the critical end point can be driven to zero temperature<sup>117</sup>. In this case, a quantum critical end point arises. The most systematic studies have been carried out in recent years in the metallic bilayer ruthenate  $\text{Sr}_3\text{Ru}_2\text{O}_7$  (ref. 118). Here, the field-tuned QCP is masked by a new, as yet unidentified, low-temperature state<sup>43,119</sup>. In ref. 120,  $\text{Sr}_3\text{Ru}_2\text{O}_7$  has been compared with the prototypical metamagnetic HF compound  $\text{CeRu}_2\text{Si}_2$ . Transport and thermodynamic measurements<sup>121</sup>, however, have proved a Landau FL state in the latter. This observation is consistent with a continuous evolution of the Fermi surface across the metamagnetic transition as inferred from recent Hall-effect and dHvA investigations<sup>122</sup>.

The related U-based HF compound  $\text{URu}_2\text{Si}_2$  shows metamagnetism around 38 T (ref. 123). However, in contrast to  $\text{CeRu}_2\text{Si}_2$ , the low-temperature magnetization indicates three subsequent first-order metamagnetic transitions as the magnetic field is increased. The first transition is related to the suppression of the as-yet-unidentified ‘hidden order’ (whose zero-field transition temperature is  $T_0 = 17.5\text{K}$ ), whereas the second and third transition points bound a phase that has been labelled ‘re-entrant hidden order’; transport experiments suggest that the latter phase hides a metamagnetic quantum-critical end point<sup>123</sup>.

## SUMMARY AND OUTLOOK

The explicit observation of antiferromagnetic QCPs in HF metals has provided the opportunity to assess the role that quantum criticality plays in the general physics of strongly correlated electron systems. Through the studies of quantum-critical HF metals, we now know that quantum criticality indeed generates NFL excitations, and does so in a robust fashion. We also know that it can lead to unconventional superconductivity.

Studies in HF metals have also elucidated the nature of quantum criticality. We now have clear evidence that quantum criticality can go beyond the standard theory of order-parameter fluctuations. The destruction of Kondo entanglement has emerged as a means of generating the inherently quantum excitations that add to the critical fluctuations of the order parameter. The evidence for such ‘Kondo collapsing’ at the QCP appears in the form of unconventional scalings, a divergence of the effective charge-carrier mass, a sudden reconstruction of the Fermi surface and the vanishing of multiple energy scales.

Still, the subject of quantum-critical HF metals is at a very early stage. Many important questions remain, and we list several here to close this review.

- We have discussed two types of quantum criticality in antiferromagnetic HF metals, one involving critical Kondo destruction and the other one being of the spin-density-wave type. Do all antiferromagnetic HF QCPs fall into one of these two categories?
- In classical critical phenomena, the identification of the critical modes—fluctuations of the order parameter—immediately leads to a field theory, the Ginzburg–Landau theory. The construction of this field theory is important for the concept of universality. For the spin-density-wave quantum critical points, the procedure is readily adapted. With the new excitations from the critical Kondo destruction, on the other hand, what is the form of the field theory?
- We have outlined the empirical evidence that the spin-density-wave type of quantum criticality promotes unconventional superconductivity. None of the materials with the clearest evidence for Kondo-destroying quantum criticality have shown superconductivity. Is this an indication of a clear-cut

correlation between the type of quantum criticality and the occurrence of superconductivity?

- What lessons can be learned from HF metals that are directly relevant to the quantum criticality of other strongly correlated systems?

doi:10.1038/nphys892

## References

1. Rosenberg, R. Why is ice slippery? *Phys. Today* **58**, 50–55 (2005).
2. Sachdev, S. *Quantum Phase Transitions* (Cambridge Univ. Press, New York, 1999).
3. Coleman, P. & Schofield, A. J. Quantum criticality. *Nature* **433**, 226–229 (2005).
4. Stewart, G. R. Non-Fermi-liquid behavior in d- and f-electron metals. *Rev. Mod. Phys.* **73**, 797–855 (2001); **78**, 743–753 (2006).
5. Löhneysen, H. v., Rosch, A., Vojta, M. & Wölfle, P. Fermi-liquid instabilities at magnetic quantum phase transitions. *Rev. Mod. Phys.* **79**, 1015–1075 (2007).
6. Löhneysen, H. v. et al. Non-Fermi-liquid behavior in a heavy-fermion alloy at a magnetic instability. *Phys. Rev. Lett.* **72**, 3262–3265 (1994).
7. Schröder, A. et al. Onset of antiferromagnetism in heavy-fermion metals. *Nature* **407**, 351–355 (2000).
8. Trovarelli, O. et al. YbRh<sub>2</sub>Si<sub>2</sub>: Pronounced non-Fermi-liquid effects above a low-lying magnetic phase transition. *Phys. Rev. Lett.* **85**, 626–629 (2000).
9. Hertz, J. A. Quantum critical phenomena. *Phys. Rev. B* **14**, 1165–1184 (1976).
10. Millis, A. J. Effect of a nonzero temperature on quantum critical points in itinerant fermion systems. *Phys. Rev. B* **48**, 7183–7196 (1993).
11. Moriya, T. & Takimoto, T. Anomalous properties around magnetic instability in heavy electron systems. *J. Phys. Soc. Jpn* **64**, 960–969 (1995).
12. Si, Q., Rabello, S., Ingersent, K. & Smith, J. L. Locally critical quantum phase transitions in strongly correlated metals. *Nature* **413**, 804–808 (2001).
13. Coleman, P., Pépin, C., Si, Q. & Ramazashvili, R. How do Fermi liquids get heavy and die? *J. Phys. Condens. Matter* **13**, R723–R738 (2001).
14. Senthil, T., Vojta, M. & Sachdev, S. Weak magnetism and non-Fermi liquids near heavy-fermion critical points. *Phys. Rev. B* **69**, 035111 (2004).
15. Andres, K., Graebner, J. E. & Ott, H. R. 4f-virtual-bound-state formation in CeAl<sub>3</sub> at low temperatures. *Phys. Rev. Lett.* **35**, 1779–1782 (1975).
16. Steglich, F. et al. Superconductivity in the presence of strong Pauli paramagnetism: CeCu<sub>2</sub>Si<sub>2</sub>. *Phys. Rev. Lett.* **43**, 1892–1896 (1979).
17. Assmus, W. et al. Superconductivity in CeCu<sub>2</sub>Si<sub>2</sub> single crystals. *Phys. Rev. Lett.* **52**, 469–472 (1984).
18. Ott, H. R., Rudiger, H., Fisk, Z. & Smith, J. L. UBe<sub>13</sub>: An unconventional actinide superconductor. *Phys. Rev. Lett.* **50**, 1595–1598 (1983).
19. Stewart, G. R., Fisk, Z., Willis, J. O. & Smith, J. L. Possibility of coexistence of bulk superconductivity and spin fluctuations in UPt<sub>3</sub>. *Phys. Rev. Lett.* **52**, 679–682 (1984).
20. Schlätzle, W. et al. Superconductivity and magnetic order in a strongly interacting Fermi system: URu<sub>2</sub>Si<sub>2</sub>. *Z. Phys. B* **62**, 171–177 (1986).
21. Grewe, N. & Steglich, F. in *Handbook on the Physics and Chemistry of Rare Earths* Vol. 14 (eds Gschneidner, K. A. Jr & Eyring, L.) 343–474 (Elsevier, Amsterdam, 1991).
22. Kondo, J. Resistance minimum in dilute magnetic alloys. *Prog. Theor. Phys.* **32**, 37–49 (1964).
23. Hewson, A. C. *The Kondo Problem to Heavy Fermions* (Cambridge Univ. Press, Cambridge, 1993).
24. Kotliar, G. & Vollhardt, D. Strongly correlated materials: Insights from dynamical mean-field theory. *Phys. Today* **57**, 53–59 (2004).
25. Doniach, S. The Kondo lattice and weak antiferromagnetism. *Physica B+C* **91**, 231–234 (1977).
26. Varma, C. M. Mixed-valence compounds. *Rev. Mod. Phys.* **48**, 219–238 (1976).
27. Seaman, C. L. et al. Evidence for non-Fermi liquid behavior in the Kondo alloy Y<sub>1-x</sub>U<sub>x</sub>Pd<sub>3</sub>. *Phys. Rev. Lett.* **67**, 2882–2885 (1991).
28. Andraka, B. & Tsvetlik, A. M. Observation of non-Fermi-liquid behavior in U<sub>0.2</sub>Y<sub>0.8</sub>Pd<sub>3</sub>. *Phys. Rev. Lett.* **67**, 2886–2889 (1991).
29. Chakravarty, S., Halperin, B. I. & Nelson, D. R. Two-dimensional quantum Heisenberg antiferromagnet at low temperatures. *Phys. Rev. B* **39**, 2344–2371 (1989).
30. Continentino, M. A., Japiassu, G. M. & Troper, A. Critical approach to the coherence transition in Kondo lattices. *Phys. Rev. B* **39**, 9734–9737 (1993).
31. Senthil, T., Vishwanath, A., Balents, L., Sachdev, S. & Fisher, M. P. A. Deconfined quantum critical points. *Science* **303**, 1490–1494 (2004).
32. Si, Q., Rabello, S., Ingersent, K. & Smith, J. L. Local fluctuations in quantum critical metals. *Phys. Rev. B* **68**, 115103 (2003).
33. Burdin, S., Grepel, D. R. & Georges, A. Heavy-fermion and spin-liquid behavior in a Kondo lattice with magnetic frustration. *Phys. Rev. B* **66**, 045111 (2002).
34. Steglich, F. in *Festkörperprobleme (Adv. Solid State Physics)* Vol. XVII (ed. Treusch, J.) 319–350 (Vieweg, Braunschweig, 1977).
35. Melnikov, V. I. Thermodynamics of the Kondo problem. *Sov. Phys. JETP Lett.* **35**, 511–515 (1982).
36. Zhu, J.-X., Grepel, D. R. & Si, Q. Continuous quantum phase transition in a Kondo lattice model. *Phys. Rev. Lett.* **91**, 156404 (2003).
37. Glossop, M. T. & Ingersent, K. Magnetic quantum phase transition in an anisotropic Kondo lattice. *Phys. Rev. Lett.* **99**, 227203 (2007).
38. Zhu, J.-X., Kirchner, S., Bulla, R. & Si, Q. Zero-temperature magnetic transition in an easy-axis Kondo lattice model. *Phys. Rev. Lett.* **99**, 227204 (2007).
39. Zhu, L., Garst, M., Rosch, A. & Si, Q. Universally diverging Grüneisen parameter and the magnetocaloric effect close to quantum critical points. *Phys. Rev. Lett.* **91**, 066404 (2003).
40. Garst, M. & Rosch, A. Sign change of the Grüneisen parameter and magnetocaloric effect near quantum critical points. *Phys. Rev. B* **72**, 205129 (2005).
41. Küchler, R. et al. Divergence of the Grüneisen ratio at quantum critical points in heavy fermion metals. *Phys. Rev. Lett.* **91**, 066405 (2003).
42. Küchler, R. et al. Quantum criticality in the cubic heavy-fermion system CeIn<sub>3-x</sub>Sn<sub>x</sub>. *Phys. Rev. Lett.* **96**, 256403 (2006).
43. Gegenwart, P., Weickert, F., Garst, M., Perry, R. S. & Maeno, Y. Metamagnetic quantum criticality in Sr<sub>3</sub>Ru<sub>2</sub>O<sub>7</sub> studied by thermal expansion. *Phys. Rev. Lett.* **96**, 136402 (2006).
44. Gegenwart, P. et al. Multiple energy scales at a quantum critical point. *Science* **315**, 969–971 (2007).
45. Zhu, L. *Quantum Phase Transitions in Strongly Correlated Metals*. Thesis, Rice Univ. (2005).
46. Pépin, C. Fractionalization and Fermi-surface volume in heavy-fermion compounds: The case of YbRh<sub>2</sub>Si<sub>2</sub>. *Phys. Rev. Lett.* **94**, 066402 (2005).

47. Küchler, R. *et al.* Grüneisen ratio divergence at the quantum critical point in  $\text{CeCu}_{6-x}\text{Ag}_x$ . *Phys. Rev. Lett.* **93**, 096402 (2004).
48. Varma, C. M., Littlewood, P. B., Schmitt-Rink, S., Abrahams, E. & Ruckenstein, A. E. Phenomenology of the normal state of Cu–O high temperature superconductors. *Phys. Rev. Lett.* **63**, 1996–1999 (1989).
49. Aronson, M. C. *et al.* Non-Fermi-liquid scaling of the magnetic response in  $\text{UCu}_{5-x}\text{Pd}_x$  ( $x = 1, 1.5$ ). *Phys. Rev. Lett.* **75**, 725–728 (1995).
50. Stockert, O., Löhneysen, H. v., Rosch, A., Pyka, N. & Loewenhaupt, M. Two-dimensional fluctuations at the quantum critical point of  $\text{CeCu}_{6-x}\text{Au}_x$ . *Phys. Rev. Lett.* **80**, 5627–5630 (1998).
51. Gegenwart, P., Custers, J., Tokiwa, Y., Geibel, C. & Steglich, F. Ferromagnetic quantum critical fluctuations in  $\text{YbRh}_2\text{Si}_2$  ( $\text{Si}_{0.95}\text{Ge}_{0.05}$ )<sub>2</sub>. *Phys. Rev. Lett.* **94**, 076402 (2005).
52. Misawa, T., Yamaji, Y. & Imada, M.  $\text{YbRh}_2\text{Si}_2$ : Quantum tricritical behavior in itinerant electron systems. Preprint at <<http://arxiv.org/abs/cond-mat/0710.3260>> (2007).
53. Sichelschmidt, J., Ivanshin, V. A., Ferstl, J., Geibel, C. & Steglich, F. Low temperature electron spin resonance of the Kondo ion in a heavy fermion metal:  $\text{YbRh}_2\text{Si}_2$ . *Phys. Rev. Lett.* **91**, 156401 (2003).
54. Kadowaki, H. *et al.* Quantum critical point of an itinerant antiferromagnet in a heavy fermion. *Phys. Rev. Lett.* **96**, 016401 (2006).
55. Custers, J. *et al.* The break-up of heavy electrons at a quantum critical point. *Nature* **424**, 524–527 (2003).
56. Gegenwart, P. *et al.* Breakup of heavy fermions on the brink of phase A in  $\text{CeCu}_2\text{Si}_2$ . *Phys. Rev. Lett.* **81**, 1501–1504 (1998).
57. Hlubina, R. & Rice, T. M. Resistivity as a function of temperature for models with hot spots on the Fermi surface. *Phys. Rev. B* **51**, 9253–9260 (1995).
58. Rosch, A. Interplay of disorder and spin fluctuations in the resistivity near a quantum critical point. *Phys. Rev. Lett.* **82**, 4280–4283 (1999).
59. Sereni, J. *et al.* Scaling the  $C \propto T \ln T$  dependence in Ce-systems. *Physica B* **230–232**, 580–582 (1997).
60. Paschen, S. *et al.* Hall-effect evolution across a heavy-fermion quantum critical point. *Nature* **432**, 881–885 (2004).
61. Norman, M. R., Si, Q., Bazaliy, Ya. B. & Ramazashvili, R. Hall effect in nested antiferromagnets near the quantum critical point. *Phys. Rev. Lett.* **90**, 116601 (2003).
62. Lee, M., Husmann, A., Rosenbaum, T. F. & Aeppli, G. High resolution study of magnetic ordering at absolute zero. *Phys. Rev. Lett.* **92**, 187201 (2004).
63. Shishido, H., Settai, R., Harima, H. & Onuki, Y. A drastic change of the Fermi surface at a critical pressure in  $\text{CeRhIn}_5$ : dHvA study under pressure. *J. Phys. Soc. Jpn* **74**, 1103–1106 (2005).
64. Park, T. *et al.* Hidden magnetism and quantum criticality in the heavy fermion superconductor  $\text{CeRhIn}_5$ . *Nature* **440**, 65–68 (2006).
65. Paul, I., Pépin, C. & Norman, M. R. Kondo breakdown and hybridization fluctuations in the Kondo–Heisenberg lattice. *Phys. Rev. Lett.* **98**, 026402 (2007).
66. Yeh, A. *et al.* Quantum phase transition in a common metal. *Nature* **419**, 459–462 (2002).
67. Bud'ko, S. L., Morosan, E. & Canfield, P. C. Magnetic field induced non-Fermi liquid behavior in  $\text{YbAgGe}$  single crystals. *Phys. Rev. B* **69**, 014415 (2004).
68. Bud'ko, S. L., Zapf, V., Morosan, E. & Canfield, P. C. Field-dependent Hall effect in single-crystal heavy fermion  $\text{YbAgGe}$  below 1 K. *Phys. Rev. B* **72**, 172413 (2005).
69. Tokiwa, Y. *et al.* Low-temperature thermodynamic properties of the heavy-fermion compound  $\text{YbAgGe}$  close to the field-induced quantum critical point. *Phys. Rev. B* **73**, 094435 (2006).
70. Onishi, Y. & Miyake, K. Enhanced valence fluctuations caused by f–c Coulomb interaction in Ce-based heavy electrons: Possible origin of pressure-induced enhancement of superconducting transition temperature in  $\text{CeCu}_2\text{Ge}_2$  and related compounds. *J. Phys. Soc. Jpn* **69**, 3955–3964 (2000).
71. Jaccard, D., Behnia, K. & Sierro, J. Pressure-induced heavy fermion superconductivity in  $\text{CeCu}_2\text{Ge}_2$ . *Phys. Lett. A* **163**, 475–480 (1992).
72. Yuan, H. Q. *et al.* Observation of two distinct superconducting phases in  $\text{CeCu}_2\text{Si}_2$ . *Science* **302**, 2104–2107 (2003).
73. Sato, N. K. *et al.* Strong coupling between local moments and superconducting ‘heavy’ electrons in  $\text{UPd}_2\text{Al}_3$ . *Nature* **410**, 340–343 (2001).
74. Saxena, S. S. *et al.* Superconductivity on the border of itinerant-electron ferromagnetism in  $\text{UGe}_2$ . *Nature* **406**, 587–592 (2000).
75. Lévy, F., Sheikin, I., Grenier, B. & Huxley, A. D. Magnetic field-induced superconductivity in the ferromagnet  $\text{URhGe}$ . *Science* **309**, 1343–1346 (2005).
76. Huy, N. T. *et al.* Superconductivity on the border of weak itinerant ferromagnetism in  $\text{UCoGe}$ . *Phys. Rev. Lett.* **99**, 067006 (2007).
77. Stockert, O. *et al.* Nature of the A phase in  $\text{CeCu}_2\text{Si}_2$ . *Phys. Rev. Lett.* **92**, 136401 (2004).
78. Stockert, O. *et al.* *Physica B* (2007, in the press).
79. Mathur, N. D. *et al.* Magnetically mediated superconductivity in heavy fermion compounds. *Nature* **394**, 39–43 (1998).
80. Scalapino, D. J., Loh, E. & Hirsch, J. E. d-wave pairing near a spin-density-wave instability. *Phys. Rev. B* **34**, 8190–8192 (1986).
81. Petrovic, C. *et al.* Heavy-fermion superconductivity in  $\text{CeCoIn}_5$  at 2.3 K. *J. Phys. Condens. Matter* **13**, L337–L342 (2001).
82. Gegenwart, P. *et al.* Non-Fermi liquid normal state of the heavy-fermion superconductor  $\text{UBe}_{13}$ . *Physica C* **408–410**, 157–160 (2004).
83. Anderson, P. W. Is there glue in cuprate superconductors? *Science* **316**, 1705–1707 (2007).
84. Yamamoto, S. J. & Si, Q. Fermi surface and antiferromagnetism in the Kondo lattice: An asymptotically exact solution in  $d > 1$  dimensions. *Phys. Rev. Lett.* **99**, 016401 (2007).
85. Si, Q. Global magnetic phase diagram and local quantum criticality in heavy fermion metals. *Physica B* **378**, 23–27 (2006).
86. Settai, R., Takeuchi, T. & Onuki, Y. Recent advances in Ce-based heavy-fermion superconductivity and Fermi surface properties. *J. Phys. Soc. Jpn* **76**, 051003 (2007).
87. Gegenwart, P. *et al.* Magnetic-field induced quantum critical point in  $\text{YbRh}_2\text{Si}_2$ . *Phys. Rev. Lett.* **89**, 056402 (2002).
88. Zhu, L. & Si, Q. Critical local moment fluctuations in the Bose–Fermi Kondo model. *Phys. Rev. B* **66**, 024426 (2002).
89. Zaránd, G. & Demler, E. Quantum phase transitions in the Bose–Fermi Kondo model. *Phys. Rev. B* **66**, 024427 (2002).
90. Vojta, M. & Kirčan, M. Pseudogapped Fermi–Bose Kondo model. *Phys. Rev. Lett.* **90**, 157203 (2003).
91. Glossop, M. T. & Ingersent, K. Numerical renormalization-group study of the Bose–Fermi Kondo model. *Phys. Rev. Lett.* **95**, 067202 (2005).
92. Kirchner, S. & Si, Q. Scaling and enhanced symmetry at the quantum critical point of the sub-Ohmic Bose–Fermi Kondo model. *Phys. Rev. Lett.* **100**, 026403 (2008).
93. Maebashi, H., Miyake, K. & Varma, C. M. Undressing the Kondo effect near the antiferromagnetic quantum critical point. *Phys. Rev. Lett.* **95**, 207207 (2005).
94. Rech, J., Coleman, P., Zaránd, G. & Parcollet, O. Schwinger Boson approach to the fully screened Kondo model. *Phys. Rev. Lett.* **96**, 016601 (2006).
95. Knebel, G., Aoki, D., Braithwaite, D., Salce, B. & Flouquet, J. Coexistence of antiferromagnetism and superconductivity in  $\text{CeRhIn}_5$  under high pressure and magnetic field. *Phys. Rev. B* **74**, 020501 (2006).
96. Paglionie, J. *et al.* Field-induced quantum critical point in  $\text{CeCoIn}_5$ . *Phys. Rev. Lett.* **91**, 246405 (2003).
97. Bianchi, A., Movshovich, R., Vekhter, I., Pagliuso, P. G. & Sarrao, J. L. Avoided antiferromagnetic order and quantum critical point in  $\text{CeCoIn}_5$ . *Phys. Rev. Lett.* **91**, 257001 (2003).
98. Singh, S. *et al.* Probing the quantum critical behavior in  $\text{CeCoIn}_5$  via Hall effect measurements. *Phys. Rev. Lett.* **98**, 057001 (2007).
99. Donath, J. G., Gegenwart, P., Steglich, F., Bauer, E. D. & Sarrao, J. L. Dimensional crossover of quantum critical behavior in  $\text{CeCoIn}_5$ . Preprint at <<http://arxiv.org/abs/cond-mat/0704.0506>> (2007).
100. Pham, L. D., Park, T., Maquilon, S., Thompson, J. D. & Fisk, Z. Reversible tuning of the heavy-fermion ground state in  $\text{CeCoIn}_5$ . *Phys. Rev. Lett.* **97**, 056404 (2006).
101. Gegenwart, P. *et al.* Non-Fermi liquid effects at ambient pressure in a stoichiometric heavy-fermion compound with very low disorder:  $\text{CeNi}_2\text{Ge}_2$ . *Phys. Rev. Lett.* **82**, 1293 (1999).
102. Loidl, A. *et al.* Local-moment and itinerant antiferromagnetism in the heavy-fermion system  $\text{Ce}(\text{Cu}_{1-x}\text{Ni}_x)_2\text{Ge}_2$ . *Ann. Phys.* **1**, 78–91 (1992).
103. Knafo, W. *et al.* Anomalous scaling behavior of the dynamical spin susceptibility of  $\text{Ce}_{0.925}\text{La}_{0.075}\text{Ru}_2\text{Si}_2$ . *Phys. Rev. B* **70**, 174401 (2004).
104. Montfrooij, W. *et al.* Non-local quantum criticality in  $\text{Ce}(\text{Ru}_{1-x}\text{Fe}_x)_2\text{Ge}_2$  ( $x = x_c = 0.77$ ). *Phys. Rev. Lett.* **91**, 087202 (2003).
105. Heuser, K., Scheidt, E.-W., Schreiner, T. & Stewart, G. R. Disappearance of hyperscaling at low temperatures in non-Fermi liquid  $\text{CeCu}_{5.2}\text{Ag}_{0.8}$ . *Phys. Rev. B* **58**, 15959–15961 (1998).
106. Stockert, O., Enderle, M. & Löhneysen, v. H. Magnetic fluctuations at a field-induced quantum phase transition. *Phys. Rev. Lett.* **99**, 237203 (2007).
107. Westerkamp, T. *et al.* *Physica B* (2007, in the press).
108. Brando, M. *et al.* (in the press).
109. Belitz, D., Kirkpatrick, T. R. & Vojta, T. How generic scale invariance influences quantum and classical phase transitions. *Rev. Mod. Phys.* **77**, 579–632 (2005).
110. Abanov, A. & Chubukov, A. V. Spin-fermion model near the quantum critical point: One-loop renormalization group results. *Phys. Rev. Lett.* **84**, 5608–5611 (2000).
111. Süllov, S., Aronson, M. C., Rainford, B. D. & Haen, P. Doniach phase diagram, revisited: From ferromagnet to Fermi liquid in pressurized  $\text{CeRu}_2\text{Ge}_2$ . *Phys. Rev. Lett.* **82**, 2963–2966 (1999).
112. Sidorov, V. A. *et al.* Magnetic phase diagram of the ferromagnetic Kondo-lattice compound  $\text{CeAgSb}_2$  up to 80 kbar. *Phys. Rev. B* **67**, 22419 (2003).
113. Lonzarich, G. G. in *Electron* (ed. Springford, M.) Ch. 6, 109–147 (Cambridge Univ. Press, Cambridge, 1997).
114. Doiron-Leyraud, N. *et al.* Fermi-liquid breakdown in the paramagnetic phase of a pure metal. *Nature* **425**, 595–599 (2003).
115. Uhlarz, M., Pfeleiderer, C. & Hayden, S. M. Quantum phase transitions in the itinerant ferromagnet  $\text{ZrZn}_2$ . *Phys. Rev. Lett.* **93**, 256404 (2004).
116. Pedrazzini, P. *et al.* Metallic state in cubic FeGe beyond its quantum phase transition. *Phys. Rev. Lett.* **98**, 047204 (2007).
117. Millis, A. J., Schofield, A. J., Lonzarich, G. G. & Grigera, S. A. Metamagnetic quantum criticality in metals. *Phys. Rev. Lett.* **88**, 217204 (2002).
118. Grigera, S. A. *et al.* Magnetic field-tuned quantum criticality in the metallic ruthenate  $\text{Sr}_3\text{Ru}_2\text{O}_7$ . *Science* **294**, 329–332 (2001).
119. Grigera, S. A. *et al.* Disorder-sensitive phase formation linked to metamagnetic quantum criticality. *Science* **306**, 1154–1157 (2004).
120. Flouquet, J., Haen, P., Raymond, S., Aoki, D. & Knebel, G. Itinerant metamagnetism of  $\text{CeRu}_2\text{Si}_2$ : Bringing out the dead. Comparison with the new  $\text{Sr}_3\text{Ru}_2\text{O}_7$  case. *Physica B* **319**, 251–261 (2002).
121. Weickert, F. *et al.* Search for a quantum critical end-point in  $\text{CeRu}_2(\text{Si}_{1-x}\text{Ge}_x)_2$ . *Physica B* **359**, 68–70 (2005).
122. Daou, R., Bergemann, C. & Julian, S. R. Continuous evolution of the Fermi surface of  $\text{CeRu}_2\text{Si}_2$  across the metamagnetic transition. *Phys. Rev. Lett.* **96**, 026401 (2006).
123. Kim, K. H., Harrison, N., Jaime, M., Boebinger, G. S. & Mydosh, J. A. Magnetic-field-induced quantum critical point and competing order parameters in  $\text{URu}_2\text{Si}_2$ . *Phys. Rev. Lett.* **91**, 256401 (2003).
124. Oeschler, N. *et al.* *Physica B* (2007, in the press).
125. Gegenwart, P. *et al.* *Physica B* (2007, in the press).
126. Friedemann, S. *et al.* *Physica B* (2007, in the press).
127. Tokiwa, Y. *et al.* Field-induced suppression of the heavy-fermion state in  $\text{YbRh}_2\text{Si}_2$ . *Phys. Rev. Lett.* **94**, 226402 (2005).

## Acknowledgements

We would like to thank E. Abrahams, C. J. Bolech, M. Brando, M. T. Glossop, S. Kirchner, M. Nicklas, P. Nikolic, S. Paschen, T. Westerkamp, S. Wirth and S. J. Yamamoto for their input on the manuscript. The work at Göttingen and Dresden has been supported in part by the DFG Research Unit 960 (‘Quantum Phase Transitions’) and the work at Rice by NSF Grant No. DMR-0706625 and the Robert A. Welch Foundation. Correspondence and requests for materials should be addressed to Q.S.